OH-Stretch Vibrational Relaxation of HOD in Liquid to Supercritical D_2O[†]

Dirk Schwarzer,*,[‡] Jörg Lindner,[§] and Peter Vöhringer[§]

Max-Planck-Institut für biophysikalische Chemie, Am Fassberg 11, D-37077 Göttingen, Germany, and Institut für Physikalische und Theoretische Chemie, Universität Bonn, Wegelerstrasse 12, D-53115 Bonn, Germany

Received: June 7, 2005; In Final Form: July 26, 2005

The population relaxation of the OH-stretching vibration of HOD diluted in D_2O is studied by time-resolved infrared (IR) pump−probe spectroscopy for temperatures of up to 700 K in the density range $12 \leq \rho \leq 58$ mol/L. For selected state points of the fluid solution, transient IR spectra were recorded following resonant excitation of the $v = 0 \rightarrow 1$ OH stretching transition with a 200 fs laser pulse centered at ~3500 cm^{-1}. Above 400 K these spectra show no indication of spectral diffusion after pump−probe delays of 0.3 ps. Over nearly the entire density range and for sufficiently high temperatures ($T > 360$ K), the vibrational relaxation rate constant, k_r, is strictly proportional to the dielectric constant, ϵ, of water. Together with existing molecular dynamics simulations, this result suggests a simple linear dependence of k_r on the number of hydrogen-bonded D_2O molecules. It is shown that, for a given temperature, an isolated binary collision model is able to adequately describe the density dependence of vibrational energy relaxation even in hydrogen-bonded fluids. However, dynamic hydrogen bond breakage and formation is a source of spectral diffusion and affects the nature of the measured k_r. For sufficiently high temperatures when spectral diffusion is much faster than energy transfer, the experimentally observed decays correspond to ensemble averaged population relaxation rates. In contrast, when spectral diffusion and vibrational relaxation occur on similar time scales, as is the case for ambient conditions, deviations from the linear $k_r(\epsilon)$ relation occur because the long time decay of the $v = 1$ population is biased to slower relaxing HOD molecules that are only weakly connected to the hydrogen bond network.

1. Introduction

The anomalous behavior of many thermodynamic properties of liquid water can be attributed to strong hydrogen bond interactions which couple the polar molecules to a complex three-dimensional random network. Therefore, a detailed molecular-level understanding of the peculiar properties of this fascinating liquid calls for experiments that are sensitive to molecular dynamics within this hydrogen-bonded network, preferably directly in the time domain.[1−3]

Fortunately, the noncovalent association of molecules has a strong influence on the spectral properties of water. In particular, the vibrational spectra of liquid water such as the infrared absorption spectrum in the intramolecular OH stretching region reflects both a distribution of hydrogen-bond strengths and a size distribution of hydrogen-bonded water aggregates in the dynamically fluctuating network. For example, the localized OH stretch absorption band of HOD in D_2O is red shifted by ~300 cm^{-1} with respect to its spectral position in the gas phase. Its enormous width of 235 cm^{-1} is mainly the result of line broadening mechanisms that can be traced back to fluctuations of the HOD coordination number and the HOD−D_2O intermolecular distances. The connection between the intermittent rearrangements and interconversions of local hydrogen-bonded configurations and the stochastic excursions of the vibrational frequency of an individual OH oscillator is termed "spectral diffusion". In the room-temperature liquid, this intriguing phenomenon is believed to be ultrafast in nature with typical time scales ranging from several tens of femtoseconds to about a picosecond.[4−14]

Similar to vibrational dephasing, intermolecular energy transfer, or vibrational energy relaxation (VER), is also governed by hydrogen bonding. On one hand, this is simply because the relaxation rate is determined by the external fluctuating solvent force acting on the excited vibrational coordinate. The stronger the coupling to the solvent, the faster is the damping of the oscillator. On the other hand, hydrogen bond-induced spectral diffusion is equivalent to a stochastic modulation of the vibrational energy gaps of an initially excited molecule. It can therefore facilitate quantum transitions by bringing about instantaneous resonances between pairs of excitations on neighboring particles. In neat liquids, intermolecular resonances are ubiquitous and are responsible for an ultrafast delocalization of vibrational excitations in both bending and stretching coordinates.[15−20]

Vibrational energy relaxation of the OH stretching mode of HOD in D_2O has been the subject of numerous experimental[4,6,16,21−28] and theoretical investigations.[29−32] In the experiments femtosecond-IR-laser pulses around 3400 cm^{-1} were used to populate the $v = 1$ state of the OH stretch. The VER rate was determined by time-resolving the excited state and/or the ground-state populations either through absorption or through Raman scattering of a delayed probe pulse. The different detection schemes fail to converge on a precise value for the lifetime, τ_r, of the OH excited state. However, τ_r seems to lie somewhere between 0.5 and 1.0 ps, which is very close to the time scale estimated for spectral diffusion of the OH stretch. Therefore, the broad scatter of the experimental values for τ_r is likely to originate from a distribution of hydrogen-

[†] Part of the special issue "Jürgen Troe Festschrift".
* To whom correspondence should be addressed.
[‡] Max-Planck-Institut für biophysikalische Chemie.
[§] Universität Bonn.

10.1021/jp0530350 CCC: $33.50
Published on Web 09/28/2005

bonded HOD−$(D_2O)_n$ configurations, which appear to be partially inhomogeneous on the time scale of VER. In fact, a recent time-resolved anti-Stokes Raman study by the Dlott group[23] suggests that the relaxation is faster for a subensemble of weakly hydrogen-bonded OH-oscillators absorbing on the blue edge of the steady-state absorption band ($\tau_r \sim 0.5$ ps) as compared to a subensemble engaged in stronger hydrogen bonds that were excited on the red edge ($\tau_r \sim 0.8$ ps).

The dependence of the OH vibrational lifetime on the strength of the hydrogen bond network was further examined by Bakker and co-workers in the temperature range $T = 30-363$ K.[22,25] For a room temperature sample, these authors found pronounced contributions of spectral diffusion to the transient absorption at early times, making a reliable extraction of the OH vibrational lifetime possible only for pump−probe delays larger than 1 ps. The temperature dependence of τ_r showed remarkable features. Just around the melting point, vibrational relaxation in ice is twice as fast as in the liquid. Further heating of the liquid to its boiling temperature increases τ_r by barely 20% from 740 to 900 fs. For a conventional liquid, the opposite temperature dependence is actually expected. Using simple arguments from isolated binary collision (IBC) theory and neglecting for the moment the weak temperature dependence of the liquid density, the collision frequency should increase linearly with $\sqrt{T}$, and hence, τ_r is expected to decrease upon raising the temperature. On the other hand, an increasing temperature will weaken the hydrogen-bonded network of liquid water, which may overcompensate for the effect of an enhanced collision frequency.

Bakker and co-workers[22,25] further interpreted the strong correlation of τ_r with the (hydrogen-bond induced) red-shift of the OH-stretch frequency with an intermolecular hydrogen-bond vibration (OH···O) acting as the accepting mode for an initially prepared OH stretching excitation.[33] Since the strength of the hydrogen bond decreases with increasing temperature, the coupling to the OH···O mode is reduced resulting in an extended OH lifetime. Note, however, that such data are also consistent with a smaller number of hydrogen bonds in which the relaxing HOD molecule is engaged at elevated temperatures. This particular aspect has been disregarded in recent studies of the vibrational relaxation dynamics of liquid water.

For this reason and to clarify the influence of the effective solvent coordination number, we substantially extend the temperature range for investigating the vibrational relaxation of HOD to above the critical point ($T_c = 643.9$ K, $\rho_c = 17.78$ mol/L, $p_c = 213.9$ bar) of the solvent, D_2O. By variation of the pressure between 1 and 1300 bar, an overall density range of 12−58 mol/L is covered. Pressure and temperature dependent experiments in supercritical fluids have been highly instrumental in the past in elucidating the mechanisms of vibrational energy relaxation.[34−38] This is because, under supercritical conditions, the density can be smoothly and continuously changed from that of a pure gas phase to densities reminiscent of a liquid phase while avoiding the otherwise perturbing gas-to-liquid phase transition. Interestingly, it was demonstrated that VER of highly vibrationally excited organic solutes in supercritical nonassociating fluids can be interpreted quantitatively from gas phase to liquidlike densities in terms of the simple and intuitive IBC model.[34,35] However, systematic pressure-, temperature-, and density-dependent studies of VER in hydrogen-bonded fluids like water do not exist so far. It is therefore a highly interesting question whether theoretical descriptions based on the assumption of isolated binary collisions can deliver reasonably accurate predictions for VER rates of such complex solute−solvents systems. We note in passing that both neutron diffraction[39,40] and atomistic computer simulations[41,42] indicate that above T_c the hydrogen bond network is considerably destabilized. At lower densities around the critical point, free water molecules and small clusters of dimers and trimers dominate, whereas at higher densities more extended structures appear. Nonetheless, we stress that hydrogen bonds are still present under supercritical conditions; their lifetime, however, is drastically reduced with respect to ambient conditions.

2. Experimental Section

Femtosecond pump−probe measurements were performed with a tunable dual-color midinfrared source and frequency-selective detection. A semi-commercial oscillator/regenerative amplifier system capable of generating 780 nm, 250 fs optical pulses with energies of 800 μJ and a repetition rate of 1 kHz pumped two optical parametric generators/amplifiers (TOPAS, Light Conversion) with a power ratio of 2:1. Pairs of tunable mid-IR pulses tunable from 1250 to 3800 cm^{-1} with a bandwidth of $\sim$120 cm^{-1} were obtained from difference frequency mixing of the two TOPAS outputs. Depending on pump power and mid-infrared wavelength, pulse energies were between 0.5 and 7 μJ, the cross-correlation time between pump and probe pulses is about 200 fs in all experiments.

Three beams (e.g., pump, probe, and reference beam) were focused into the sample with an effective focal length $f = 100$ mm off-axis parabolic mirror. Pump pulses taken from the TOPAS with the higher output were sent through a motorized optical delay line (Nanomover, Melles Griot) and through a tunable half wave retardation plate. The pump frequency was adjusted to $\sim$3500 cm^{-1} for exciting the OH stretch vibration. The output of the TOPAS generating the probe wavelength was attenuated with a combination of tunable half-wave plate and wire-grid polarizer to less than 10% of the pump energy and was then split into two beams (probe and reference) of equal intensity. Only the probe pulse was directed through an optical delay line, while the reference beam was forwarded directly to the sample such that it preceded the pump and probe beams by 1 ns. Behind the sample, all three beams were collimated with another $f = 100$ mm off-axis parabolic mirror. While the remaining pump light was captured in a beam dump, probe and reference signals were focused with CaF_2 lenses onto the entrance slits of a monochromator and detected at the exit with a commercial dual row MCT array detector system. All measurements were taken with the polarizations between pump and probe pulses set to magic angle.

The fluid samples were prepared in a high-temperature high-pressure cell, which can operate up to 1500 bar at 750 K. Our design differed from previous approaches[43,44] in that the path length of the cell had to be in the range of only 100−500 μm. The cell body was made of the nickel-based high-temperature alloy. Its length and outer diameter were 62 and 50 mm, respectively. Sapphire disks of 5 mm diameter and 2.50 mm thickness were employed as optical windows. The clear aperture of the sample cell was 2.5 mm. Four heating cartridges with a maximum power of 1 kW were embedded into the cell body to heat the sample above T_c of water. The cell had three inlets, one of which was used as a lead-through of a thermocouple for monitoring and controlling the temperature inside the cell with an accuracy of ± 1 K. The other two were used to load the cell with the initially liquid HOD/D_2O mixture. Pressure was measured with an accuracy of 1% by a manometer connected to the cell. The high-pressure cell was also used to measure OH-stretch absorption spectra of HOD in D_2O under similar conditions as in the time-resolved experiments.

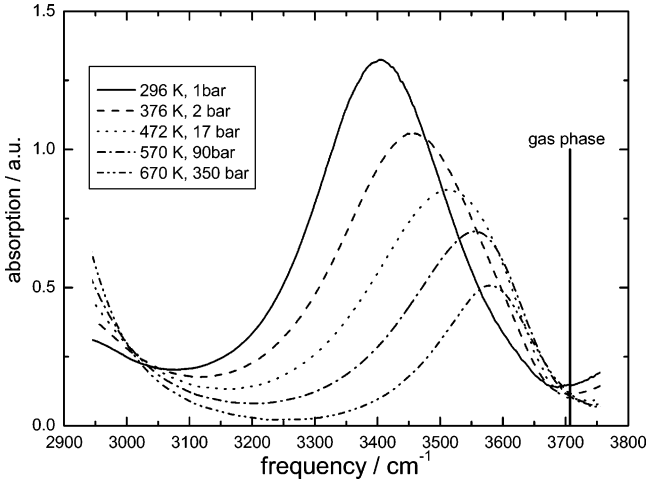

Figure 1. Linear absorption spectra of 2% HOD in D_2O in the OH stretch region at various temperatures. The state points correspond to densities of 55.4, 53.1, 48.1, 40.0, and 27.3 mol/L (ordered with increasing temperature).

HOD solutions were prepared by mixing D_2O with 1−5% H_2O. For the time-resolved experiments, the sample concentration and optical path length inside the cell was adjusted to produce a peak optical density between 0.5 and 1.0.

Density and dielectric constant for various thermodynamic state points of water were calculated from pressure and temperature data using the PROPATH program package.[45]

3. Results

The destabilization of the hydrogen bond network with increasing temperature and decreasing density can be readily illustrated by the OH stretch absorption spectrum as presented in Figure 1. The spectra were recorded for a constant HOD concentration of 2% and a constant sample length of 0.2 mm. Since the density changes upon a temperature and/or pressure variation, the HOD concentration per unit volume also changes. To correct for this effect, the spectra were multiplied by a factor ρ_{amb}/ρ_i, where ρ_{amb} and ρ_i correspond to the density at ambient conditions and at the state point i, respectively, Hence, the spectra displayed in Figure 1 correspond to density-dependent spectra renormalized to constant HOD concentration. The center of the OH band of HOD shifts from 3404 cm^{-1} at ambient conditions to 3556 cm^{-1} at 570 K when moving along the gas−liquid coexistence curve. It further shifts to the blue and reaches 3580 cm^{-1} above the critical temperature at 670 K and 350 bar. At the same time, the spectrum narrows from 235 to 160 cm^{-1} and the oscillator strength reduces by 73% when going from ambient to supercritical conditions. Yet there is still considerable overlap between all the spectra. More importantly, a large gap exists between the spectral positions of the supercritical spectrum and of the pure gas-phase spectrum, which is located at 3704 cm^{-1}. This finding clearly indicates that hydrogen bonds are still present even at the lowest density shown in Figure 1. These observations are in complete agreement with earlier investigations of the OH and OD stretch spectrum of HOD in water.[46,47]

In Figures 2 and 3, results from time-resolved experiments at 398 K and 500 bar are presented. Under these conditions, the D_2O density is 53.4 mol/L and only 4% below its value under ambient conditions. Figure 2 shows transient absorption spectra of the OH stretching vibration at six different pump−probe delay times. The excitation frequency of the pump pulse was always centered at 3530 cm^{-1} whereas the probe frequency

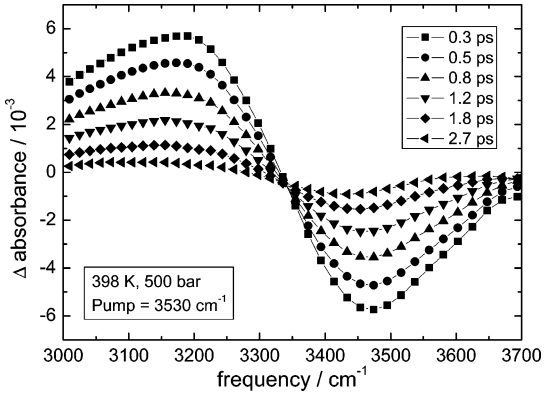

Figure 2. Transient vibrational spectra of 2% HOD in D_2O at 398 K and 500 bar ($\rho = 53.4$ mol/L) after excitation with a laser pulse centered at 3530 cm^{-1}. Spectra are shown for different pump−probe delays.

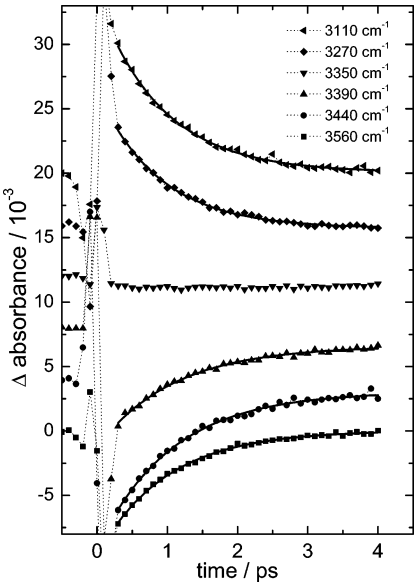

Figure 3. Time dependent induced absorption signals at various probe frequencies for the same data set as shown in Figure 3 (for clarity the traces are successively shifted along the vertical axis by a constant amount). The solid lines are exponential fits for t > 0.3 ps and yield $\tau_r = 1.0$ ps.

was varied between 3100 and 3700 cm^{-1} in steps of 120 cm^{-1}. Because of the limited bandwidth of the probe pulse of only 120 cm^{-1}, narrow-band spectra with considerable overlap were first measured from which transient spectra over a broader frequency range could be constructed. Around 3470 cm^{-1}, the bleaching/stimulated emission of the $v = 0 \rightarrow 1$ OH stretching transition is observed whereas at lower frequencies, the signal is positive resulting from the induced absorption of the corresponding $v = 1 \rightarrow 2$ transition. The width of the anharmonically shifted excited-state absorption is considerably broader and strongly asymmetric as compared to the linear absorption spectrum under identical conditions. These features are known from previous time-resolved experiments on HOD/D_2O under ambient conditions.[48] However, in contrast to liquid water at room temperature, where pump-induced spectral holes were observed that broaden and shift with increasing delay (see Figure 2 in refs 6 and 48), there is no clear evidence for spectral diffusion to occur at elevated temperatures. In fact, the nearly isosbestic point at 3350 cm^{-1}, which was not observed previously for room temperature and 1 bar using pump pulses of similar wavelength and bandwidth,[6,48] suggests a simple two-state kinetic relaxation following infrared excitation. Such an

interpretation is further corroborated by the time-resolved transient absorption signals recorded at various probe frequencies (see Figure 3). For clarity, subsequent data were vertically shifted by successively adding a constant optical density of 0.008. During the temporal overlap of the pump and probe pulses (i.e., around $t = 0$), a strong coherent coupling artifact is generated by the rather thick sapphire windows of the sample call. The unperturbed absorption signal associated with OH-stretch vibrational relaxation appears for $t > 0.3$ ps. Here, the curves can be fitted perfectly by single-exponential decays with a time constant of $\tau_r = 1.0$ ps provided a small offset is included, which takes into account a slightly heated probe volume after the excess vibrational energy has been fully dissipated and equipartitioned over the nuclear degrees of freedom of the surroundings. Considering a pump pulse energy of 4 μJ and a focus diameter of about 100 μm the temperature raise can be estimated to be 1−2 K. At the maximum of the transient absorption and bleaching in Figure 2 the amplitude of the offset amounts to less than 5% of the total signal, respectively. Therefore, its influence on the evaluated time constants is negligible. In agreement with the isosbestic point seen in Figure 2, no dynamics can be detected in Figure 3 at a probe frequency of 3350 cm^{-1}. At higher temperatures, qualitatively identical spectral features were found with no indication for spectral diffusion after 0.3 ps. These observations lead to two immediate conclusions for water above ~400 K: (i) spectral diffusion is substantially faster than at room temperature and (ii) spectral diffusion proceeds much faster than the OH-stretch vibrational relaxation. In recent vibrational echo studies of HOD in D_2O at room temperature[12−14] a long tail component of spectral diffusion of 1.4 ps was found and attributed to the breaking and making of hydrogen bonds. Molecular dynamics simulations[49] suggest that this process depends on the water potential used and that it accelerates by a factor of 4−8 upon increasing the temperature from 298 to 400 K. This supports our interpretation of the isosbestic point in Figure 2 as being due to the fact that spectral diffusion is faster than vibrational relaxation.

In Figures 2 and 3, the vibrational relaxation times derived from decay of the $v = 1 \rightarrow 2$ OH stretching excited-state absorption ($\nu_{probe} = 3050-3250$ cm^{-1}) are on average 5% shorter than those determined from the ground-state recovery ($\nu_{probe} = 3450-3600$ cm^{-1}). At this stage, this difference is to close to our experimental accuracy to assign it some particular physical relevance. With further increasing temperature, the two relaxation rates indeed converge to a common singular value. It can thus be concluded that our probe wavelength dependence—if significant at all—is clearly much weaker than previously reported for liquid water in its region of thermodynamic stability at ambient pressure.[25] Therefore, the previously invoked "bottleneck" state, which is transiently populated during the relaxation thereby decelerating repopulation of the vibrational ground state, cannot be confirmed. The failure of our data to reveal an unambiguous wavelength dependence of τ_r at higher temperatures may indicate that the data from Nienhuys et al.[25] although evaluated at pump probe delay times >1 ps were yet influenced by spectral diffusion. In the following and only for the sake of consistency, we will exclusively use the ground-state recovery component for determining the temperature and density dependence of the OH vibrational relaxation rate of HOD in D_2O. Since the difference between ground-state recovery times and excited-state decay times is so small, an analysis of the transient absorption component would lead to identical conclusions.

In Figure 4, transient bleaching signals covering a density range between 23.8 and 57.1 mol/L are presented. At the same time, the temperature was varied between 322 and 697 K. For the two lowest densities, pump and probe pulses were centered at 3600 cm^{-1} while, for the remaining signals, the pulses were tuned to 3540 cm^{-1}. Note that in Figure 4 the negative pump-induced absorbance is plotted to facilitate a semilogarithmic representation of the data vs delay. The time constant, τ_r, derived from single-exponential fits increases from 0.75 ps at the highest density by almost a factor of 10 upon lowering the density by 60%. The error of τ_r below 630 K is estimated to be about 5%. Above the critical temperature, the signals suffered from increasing noise, which probably arose from the typical density fluctuations in the sample. Nevertheless, the error of τ_r under these conditions is below 10%, close to ρ_c it remained below 15%. All the vibrational relaxation times are summarized in Table 1.

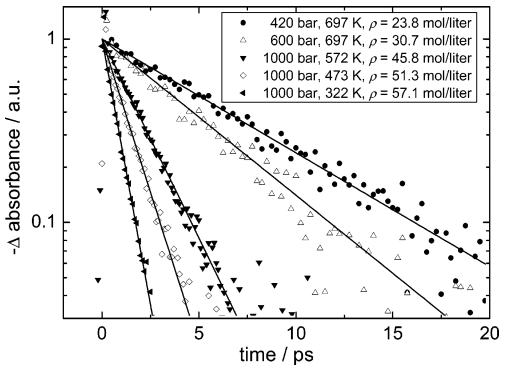

Figure 4. Normalized transient absorption signals of 2% HOD in D_2O recorded under various thermodynamic conditions. For the signals at the two lowest densities, the pump and probe pulses were centered at 3600 cm^{-1} while for the other transients, the pulse were tuned to 3540 cm^{-1}. Solid lines are single-exponential fits with time constants of τ_r = 7.0, 5.2, 2.0, 1.3, and 0.75 ps, respectively.

TABLE 1: Relaxation Times of the OH Stretch Vibration of HOD in D_2O

T/K	p/bar	ρ/mol L^{-1} [a]	ϵ[a]	τ_r/ps
297	18	55.4	78.9	0.74 ± 0.04
297	1000	57.6	82.4	0.75 ± 0.04
322	22	54.9	70.2	0.75 ± 0.04
322	1000	57.1	73.6	0.76 ± 0.04
347	14	54.2	62.6	0.84 ± 0.05
347	1004	56.4	65.7	0.77 ± 0.04
373	5	53.2	54.4	0.91 ± 0.05
373	1010	55.5	58.5	0.89 ± 0.05
398	13	52.2	49.4	1.00 ± 0.05
398	500	53.4	51.0	1.02 ± 0.06
398	1003	54.6	52.5	0.90 ± 0.05
424	7	50.9	43.8	1.19 ± 0.06
424	1000	53.5	46.9	1.12 ± 0.07
473	19	48.0	34.8	1.42 ± 0.07
473	1005	51.3	38.2	1.31 ± 0.07
523	41	44.4	27.1	1.85 ± 0.09
523	1003	48.7	31.0	1.53 ± 0.08
572	100	39.9	20.5	2.29 ± 0.12
572	1000	45.8	25.3	2.04 ± 0.11
621	1000	42.5	20.5	2.15 ± 0.11
701	320	12.7	3.24	15 ± 5
697	350	16.6	4.48	10.5 ± 1.6
697	420	23.8	7.5	7.0 ± 0.7
697	600	30.7	11.0	5.2 ± 0.5
697	800	34.2	12.9	4.3 ± 0.4
697	1000	36.4	14.2	3.8 ± 0.4
697	1260	38.5	15.5	3.3 ± 0.3

[a] Reference 45.

The strong density and temperature dependence of τ_r is summarized in Figure 5, where the relaxation rate constant, $k_r = \tau_r^{-1}$, of the OH-stretching vibration of HOD is plotted vs the

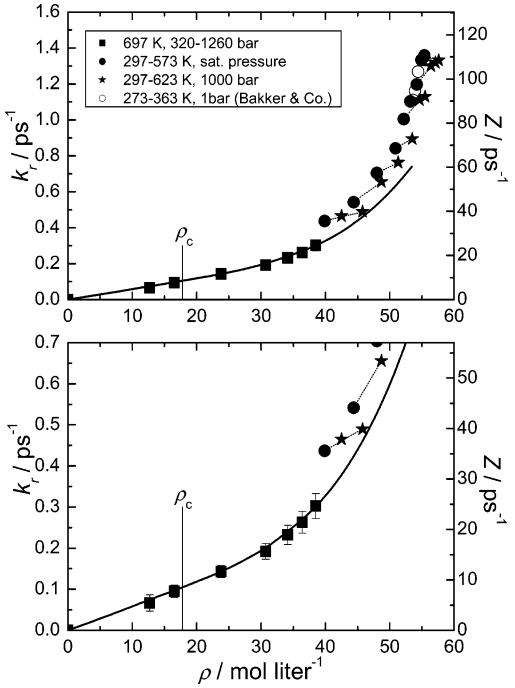

Figure 5. Density dependence of the OH-stretch relaxation rate of HOD in D_2O at various temperatures (the lower panel enlarges the low-density part, ρ_c denotes the critical density of water). Dotted lines connect isothermal rate constants below T_c at 573, 523, 473, 423, 398, and 347 K (from bottom to top). Open circles are data from refs 22 and 25. The solid line is the density dependence of the attractive hard-sphere collision frequency (note *Z*-axes on the right) calculated for a supercritical isotherm at 697 K as described in the text.

D_2O density. The lower panel zooms into the low-density region to highlight the ρ dependence of the relaxation rate along a supercritical isotherm at 697 K (filled squares). A transition from the linear $k_r(\rho)$ dependence typical for gas phase to a much steeper rise can be observed. The filled circles correspond to measurements that were carried out under subcritical conditions by simply following the temperature-dependent saturation vapor pressure of the liquid. The stars are relaxation rates obtained under isobaric conditions of 1000 bar while changing the temperature from 297 to 623 K. Hence, dotted lines connect pairs of relaxation rates determined for different densities but belonging to a mutual subcritical isotherm, i.e., the lines from bottom to top connect $k_r(\rho, 573\ K)$, $k_r(\rho, 523\ K)$, $k_r(\rho, 473\ K)$, etc. For comparison, temperature-dependent k_r values distributed between 273 and 373 K at a constant pressure of 1 bar are included by open circles and were taken from the work of Bakker and co-workers.[22,25] They agree quite well with our own data determined at low pressures and low temperatures. The top dotted line demonstrates that only 75% of the small increase of the relaxation time observed upon an atmospheric heating of water from its melting to its boiling point corresponds to a true temperature effect. The remaining 25% are simply brought about by the reduction of the sample density.

4. Discussion

In the following, we attempt to discuss the observed density and temperature dependence of the relaxation rate constant, k_r, within the framework of isolated binary collision (IBC) theory. For hydrogen-bonded fluids like water, which are normally characterized by highly anisotropic intermolecular interaction potentials, such an approach seems neither physically appropriate nor promising. However, we will see that a data analysis based on an IBC ansatz can be very helpful in unraveling the pure population dynamics uncontaminated by the dynamics of spectral diffusion via their different density and temperature dependencies.

A. Collision Model Approach for Spherical Particles. We start with a simple collision model for spherical particles to explain our $k_r(\rho)$ data under supercritical conditions. The model was used successfully to quantitatively explain the density dependence of vibrational energy relaxation of polyatomic organic solutes in supercritical fluids[34] and fluid mixtures.[35]

The basic assumptions of IBC models are that vibrational energy relaxation proceeds via binary interactions and that *P*, the relaxation probability per collision, is the same for both the gas and the liquid phase (see, e.g., ref 50 and references therein). The rate constant for a transition from level *i* to level *f* is then given by

$$k_{i,f}(\rho,T) = P_{i,f}(T)Z(\rho,T) \tag{1}$$

where the density dependence of $k_{i,f}$ is exclusively due to that of the collision frequency *Z*, whereas the temperature influences the relaxation rate through both, $P_{i,f}$ and *Z*. Apart from $P_{i,f}$, which is not easily computed and therefore is used in the following as a scaling factor, the determination of $k_r(\rho)$ at constant *T* reduces to a calculation of the appropriate density dependence of the collision frequency.

Defining a collision as an event in which two spherical particles approach each other to within a certain distance σ, the collision frequency is expressed as[51,52]

$$Z = Z_0 g(\sigma), \tag{2}$$

where $g(\sigma)$ is the value of the radial distribution function around the excited particle at distance σ and Z_0 is the usual gas-phase collision frequency

$$Z_0 = \rho\sigma^2\sqrt{\frac{8\pi k_B T}{\mu}} \tag{3}$$

To model the collision frequency of HOD in supercritical D_2O, we assume water to be a Lennard-Jones fluid; i.e., D_2O-D_2O interactions are of the type

$$V_v = 4\epsilon_v[(\sigma_v/r)^{12} - (\sigma_v/r)^6] \tag{4}$$

The potential parameters σ_v and ϵ_v are chosen such that the critical data of the Lennard-Jones fluid[53] ($T_c^* = 1.31 = k_B T_c/\epsilon_v$, $\rho_c^* = 0.31 = \rho_c\sigma_v^3$) match those of D_2O, i.e., $\sigma_v = 0.307$ nm and $\epsilon_v/k_B = 491.5$ K. An often encountered problem when using soft potentials like the Lennard-Jones interaction is to accurately specify the distance σ at which energy transferring collisions can occurs. Though for certain models this was shown to be possible in principle,[54] the accurate determination of *Z* is generally limited to hard particles. Accordingly, we assume an attractive hard-sphere (AHS) interaction between the solute HOD and the solvent D_2O, which combines the attractive part of the Lennard-Jones potential with the hard-sphere repulsion[55]

$$V_u = \infty, \quad r < \sigma_u$$

$$V_u = -\epsilon_u, \quad \sigma_u \le r \le 2^{1/6}\sigma_u$$

$$V_u = 4\epsilon_u[(\sigma_u/r)^{12} - (\sigma_u/r)^6], \quad r > 2^{1/6}\sigma_u \tag{5}$$

Well depth, ϵ_u, and diameter, σ_u, were assumed to be the same as for D_2O-D_2O interactions, i.e., $\epsilon_u = \epsilon_v$ and $\sigma_u = \sigma_v$. In this way, no adjustable parameter remained to calculate the

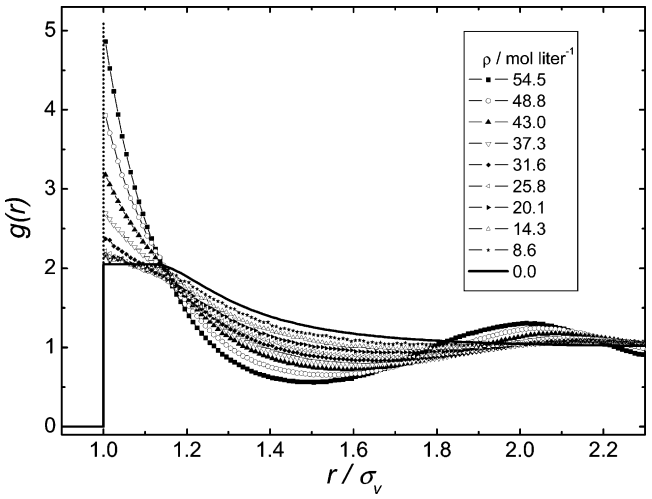

Figure 6. Radial distribution functions of an attractive hard-sphere particle in a Lennard-Jones fluid at various densities ($\epsilon_u/k_B = \epsilon_v/k_B =$ 491.5 K, $\sigma_u = \sigma_v = 0.307$ nm, $T = 697$ K).

collision frequency. Despite its simplicity, this model of an AHS particle immersed in a Lennard-Jones bath has the great advantage of reasonably resembling the fluid in terms of its compressibility and other thermodynamic parameters, in addition to allowing for an unambiguous definition of the collision frequency, Z_{AHS}, in the binary mixture.

For the calculation of radial distribution functions the Monte Carlo method was employed.[56] Simulations were performed on a canonical ensemble of 500 particles, one of which was the solute. For a constant temperature of 697 K, the corresponding results for the radial distribution function, $g(r)$, at various densities are shown in Figure 6. The solid line represents the low-density limit, i.e., $g(r) = \exp(-V_u/(k_BT))$. Above a density of 8 mol/L, marked deviations from this gas-phase distribution begin to appear. The formation of a liquidlike structure is evident from an increase of the first peak at $r/\sigma_v = 1$ and the formation of a second peak at $r/\sigma_v = 2$. At typical liquid densities, i.e., above 40 mol/L, the pronounced rise of the first peak with increasing density becomes much stronger and the width of the peak narrows. This is because molecules of the first "solvation" shell have to be packed tighter around the solute due to growing importance of the repulsive interactions with the remaining solvent. This is a typical behavior for a compressed fluid, whose collision frequency begins to display a very high sensitivity to small variations of the density (see below). The magnitude of $g(\sigma)$ right at the surface of the AHS particle was obtained from Figure 6 by extrapolation to $r/\sigma_v = 1$ (dotted line) and was used in combination with eqs 2 and 3 to calculate the collision frequency as a function of density. The solid curve shown in Figure 5 (Z_{AHS}-axis on the right) reproduces the calculation for $Z(\rho)$ at a temperature of 697 K. Projecting this result onto the OH-stretch vibrational relaxation rates obtained for HOD in supercritical D_2O at the same temperature reveals a scaling factor, $P = k_r/Z_{AHS}$, between collision frequency and relaxation rate constant of 0.012. According to eq 1, this value corresponds to the probability for an OH-stretching relaxation to occur during an HOD−D_2O binary collision. The agreement between experimental data points at 697 K and AHS collision frequency is impeccable. In particular, the stronger than linear increase of $k_r(\rho)$ above 30 mol/L is accurately reproduced by the binary collision frequency derived for an attractive hard-sphere solute immersed in a Lennard-Jones solvent.

Above densities of 40 mol/L, the AHS collision frequency clearly underestimates the relaxation rate constant. The fact that in this region the experimental data points were collected at much lower temperatures cannot be held responsible for these marked deviations. This is because for the liquid solution at constant density, the calculated AHS collision frequency increases with increasing temperature, in stark contrast to the experimentally observed T dependence of the relaxation rate. The positive temperature dependence of the AHS collision frequency results predominantly from the mean particle velocity scaling with $\sqrt{T}$, which cannot be compensated by the weak loss of amplitude of the first peak of the radial distribution function when the temperature is raised (see eq 3).

Finally, it should be mentioned that for the limited temperature intervals discussed here, the assumption of a temperature independent transition probability should be fairly reasonable In fact, if there were any dependence at all, P is expected to increase with temperature. Hence, the transition probability cannot be held responsible for the inability of the AHS model to reproduce the experimental temperature trend of the vibrational relaxation rate.

B. Dependence of k_r on Hydrogen Bond Density. While it can remarkably well account for the density dependence of the relaxation rate, the AHS collision frequency is unable to provide even a qualitative description of the temperature dependence. Apparently, this failure has to be attributed to the simplicity of the model. In particular, the tendency of water to form hydrogen bonds to nearest neighbors and the inherent anisotropy associated with the buildup of closed solvation shell structures cannot be captured at all with the oversimplifying attractive hard sphere potential. Yet, earlier investigations of the temperature and density dependence of vibrational relaxation processes in supercritical fluids[34,35,57] point to the dominant importance of the local bath density in the first solvation shell of the solute (corresponding to the first peak of the $g(r)$ in Figure 6). It was noticed that the magnitude of exactly this first peak of the radial distribution function grew to slowly to overcompensate the decreasing particle velocity with decreasing temperature. Hydrogen bonding on the other hand will indeed favor a more rapid formation of a closed solvation shell upon cooling the liquid mixture with a preference for a tetrahedral coordination of the central HOD solute once the mixture reaches the freezing point.

Lacking at this point more realistic solute−solvent interaction potentials that are able to correctly mimic the influence of hydrogen bonding on the structure of the solvent cage, one might wish to resort to more intuitive measures to describe the local density in the first solvation shell more accurately. One such measure can be the effective number of hydrogen bonds formed by the initially excited water molecule. Note that such an idea is based on the notion of a discrete size distribution of water aggregates which can coexist in the liquid and was already born with the early studies on OH-stretch relaxation of HOD in D_2O by Laenen et al.[26,27] Furthermore, such dynamical cluster models were able to provide a reasonable description of the intermolecular vibrational spectrum of liquid water near the melting point.[58] Other models, which describe k_r as a function of the length of the hydrogen bond connected to the excited OH-oscillator[6] are likely to be equivalent to cluster models simply because average cluster size and average hydrogen-bond length should be highly correlated quantities. It is quite unlikely that the two effects on the relaxation rate, i.e., the dependence on the hydrogen-bond length and the dependence on the average cluster size, will ever be unambiguously disentangled.

To identify a correlation between $k_r(\rho,T)$ and the number n_{HB} of hydrogen bonds per water molecule one has to rely on

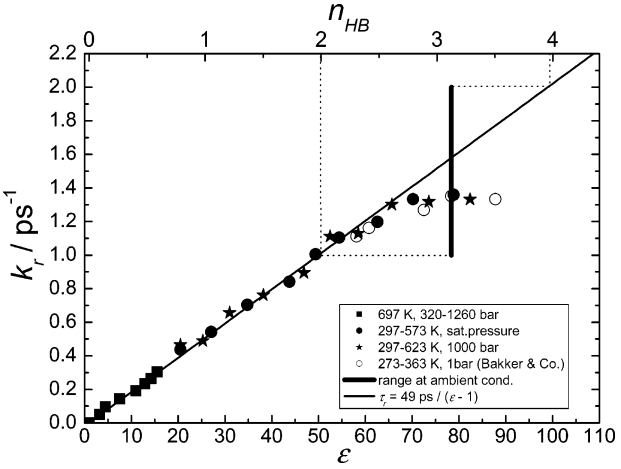

Figure 7. OH-stretch relaxation rate of HOD vs dielectric constant of water. The top axes indicates the average number of hydrogen molecules per water molecule derived from molecular dynamics simulations.[60] Open circles are data from refs 22 and 25. The thick bar assigns the range of time constants found under ambient pressure[23,28] (thin dotted lines show that the slowest and fastest rates correspond to two and 4-fold hydrogen-bonded HOD molecules, respectively).

computer simulations with realistic water models. Fortunately, such calculations for water up to supercritical conditions have already been carried out.[59,60] Here, we refer to an inspiring paper by Okazaki and co-workers,[60] who investigated the dielectric constant, ϵ, of water from ambient to supercritical conditions using a fluctuating-charge TIP4P-FQ potential model. In defining a pair of water molecules as hydrogen bonded when one of the hydrogen−oxygen distances is less than 0.25 nm and, simultaneously, the interaction energy is stronger than −17.4 kJ/mol, they found a linear correlation between n_{HB} and ϵ. The combined geometric and energetic criterion for defining hydrogen bonds turned out to be much better at high temperatures than the usual, purely geometrical one (first peak in the OH radial distribution function). This is because many water molecules, which were counted as bound in terms of their geometry had repulsive interaction energies and were obviously nonbonded.[59] The threshold energy was derived from the distribution of pair interaction energies exhibiting a low energy peak due to hydrogen-bonded neighbors, which was separated from the remainder by a minimum at about −17.4 kJ/mol.[61]

In analogy to these simulations, the vibrational relaxation rate is compared in Figure 7 directly with the experimental dielectric constant of water at the particular state point (symbols have the same meaning as in Figure 5). The top axis in Figure 7 converts the dielectric constant to the average number of hydrogen bonds per water molecule, n_{HB}, according to the results of the molecular dynamics calculations from ref 60. For the vast majority of the data points (i.e., $\epsilon < 60$ corresponding to $T > 360$ K), the diagram impressively demonstrates a *clear linear relation between the vibrational rate constant, the dielectric constant, and the number of hydrogen bonds*. Even the series of isothermal data pairs, which was clearly spread out in Figure 5 (filled cicles and stars connected by dotted lines), now collapses onto a single straight line.

In the region $1 \leq \epsilon \leq 60$, the dependence of the vibrational relaxation time on the dielectric constant can be expressed by the simple relation $\tau_r = 49 \text{ ps}/(\epsilon - 1)$ (solid line in Figure 7). For $\epsilon > 60$, the experimental points begin to deviate from this linear correlation. Their deviation however depends on how k_r was actually measured and how its precise value was retrieved from the data.

SCHEME 1: Kinetic Model of Vibrational Energy Relaxation and Spectral Diffusion

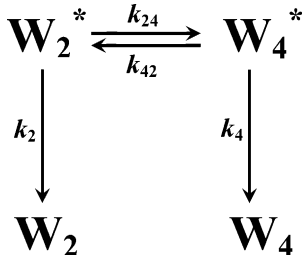

Referring to Figure 7, k_r seems to approach an asymptotic value of 1.4 ps^{-1} for large ϵ, provided the early decay of the kinetic traces was attributed to spectral diffusion and was therefore disregarded in the data analysis (this was done in refs 14, 22, and 25). This rate, derived from the OH-population decay at $t > 1$ ps, we continue to denote by k_r. In contrast, frequency resolved methods identified vibrational relaxation time which varied under ambient conditions between 0.5 and 1.0 ps when the entire kinetic traces including the early decay was analyzed.[23,28] This range is indicated in Figure 7 by a thick bar. In the next paragraph, we will discuss the origin of this data scatter in more detail.

C. Kinetic Model Including Vibrational Energy Relaxation and Spectral Diffusion. As noted before, the time scales of spectral diffusion and vibrational relaxation in liquid water at room temperature are apparently not well separated but rather, both processes appear to proceed in parallel. The fastest component of the OH-stretch relaxation in HOD/D_2O at 1 bar/298 K ($\epsilon = 78$) of ∼0.5 ps was found at the red edge of the OH-stretch band where the strongest hydrogen-bonded water molecules absorb. On the other hand, the slowest components were observed in the high frequency portion of the spectrum. Accordingly, the short lifetime was tentatively attributed to "icelike" water.[23] Such an interpretation is indeed supported by the $k_r(n_{HB})$ correlation depicted in Figure 7. Extrapolating this linear relation to an average number of hydrogen bonds of $n_{HB} = 4$ yields indeed a rate constant of (0.5 ps)$^{-1}$ in full accordance with the decay of a low-frequency subensemble. In analogy, the high-frequency subensembles exhibited rate constants of (1 ps)$^{-1}$, which according to Figure 7 are consistent with an average of 2 hydrogen bonds (see dotted lines). The question remains why k_r derived from the long time decay of the excited OH-population (1.4 ps^{-1}) is smaller than expected from the linear $k_r(\epsilon)$ or equivalently, $k_r(n_{HB})$ dependence (1.6 ps^{-1}).

To elucidate this issue a simple kinetic model is devised that involves two subensembles denoted W_2 and W_4 (Scheme 1). This simplified approach is rationalized by the recent time-resolved anti-Stokes Raman experiments of Dlott and co-workers[23] showing that the OH-stretch excited-state spectrum can indeed be decomposed into two overlapping subbands. According to Figure 7, the excited populations of W_2 and W_4 may correspond to 2- and 4-fold hydrogen-bonded HOD molecules. For the moment, 3-fold coordinated species shall be neglected but they can be incorporated in the model in a straightforward fashion. From an intuitive point of view, one may expect that the strongest damping of the OH-vibration arises from configurations were the HOD molecule is connected to the hydrogen bond network just at the OH-site. At $n_{HB} = 4$ the probability that this is the case amounts to 1, whereas at $n_{HB} = 2$ it is only 0.5 suggesting that the slower relaxing subensemble W_2 resembles those HOD molecules where the OH is not involved in hydrogen bonding. This conjecture, however, can only be confirmed by computer simulations.

In Scheme 1, spectral diffusion due to hydrogen bond breakage and formation is included by assuming a dynamic equilibrium between W_2 and W_4 described by an equilibrium constant $K_{24} = k_{42}/k_{24}$. The rate constants, k_{24} and k_{42}, are the rate constants for the forward and backward interconversion between the two aggregates. The vibrationally excited species, W_2* and W_4*, relax with their vibrational relaxation rate constants, k_2 and k_4, respectively. The kinetic model can be solved analytically and generally leads to nonexponential decays of the individual excited-state populations. The rate of spectral diffusion is equivalent to the inverse equilibration time, which is given by the sum $1/\tau_d = k_d = k_{24} + k_{42}$. Whereas the short time dynamics of the OH-stretch population decay strongly depends on which subensemble is excited by the pump and monitored by the probe pulse, the long time decay rate constant is always given by the expression

$$k_r = \frac{1}{2}(k_2 + k_{24} + k_4 + k_{42} - \sqrt{(k_2 + k_{24} - k_4 - k_{42})^2 + 4k_{24}k_{42}}). \quad (6)$$

For HOD at 1 bar and 298 K, k_r can be estimated from the available experimental data. An equilibrium constant of unity is assumed (i.e., $K_{24} = 1$ and, hence, $k_{42} = k_{24} = k_d/2$) thereby ascertaining that the number of hydrogen bonds per molecule on average is $n_{HB} = 3$ as is evidenced by Figure 7. Then, eq 6 simplifies to

$$k_r = \frac{k_2 + k_4}{2} + \frac{k_d - \sqrt{(k_2 - k_4)^2 + k_d^2}}{2}. \quad (7)$$

If spectral diffusion is much faster than vibrational relaxation, i.e., $k_d \gg k_2, k_4$, the long time decay is described exactly by the first term of eq 7 which is the weighted average (according to the appearance of W_2 and W_4) over the two individual vibrational relaxation rate constants contributing to relaxation. Generalizing this kinetic model to allow for arbitrary cluster sizes, the average rate constant becomes

$$k_r = \sum_i x_i k_i, \; k_d \gg k_i \quad (8)$$

where x_i is the mole fraction of the component, W_i, in the sample. Each component, W_i, denotes an subensemble of HOD molecule hydrogen-bonded to i D_2O particles and relaxes with its proper cluster-specific vibrational relaxation rate constant, k_i.

From Figures 2 and 3, it was concluded that spectral diffusion becomes much faster than vibrational relaxation when the temperature exceeds 400 K. Under these condition, the dielectric constant remains in the range $1 \leq \epsilon \leq 50$, and consequently, the straight line in Figure 7 reproduces ensemble averaged relaxation rate constants such as those expressed by eq 8.

In contrast, at room temperature where k_d is of the order of k_2 and k_4, the relaxation rate even at long times is influenced by k_d unless k_2 and k_4 are almost identical. Since the second term in eq 7 is always negative the apparent vibrational relaxation rate constant, k_r, is smaller than the weighted average over the cluster-specific rate constants given by eq 8. This effect can indeed be observed in Figure 7 where the relaxation rates derived from the long time decay at low temperatures ($65 < \epsilon < 90$) appear consistently below the straight line.

The difference between eqs 7 and 8 at ambient conditions can be quantified directly from the simplified kinetic model (Scheme 1) by considering only W_2 and W_4. According to Figure 7, their cluster specific relaxation rates are $k_2 = 1$ ps^{-1} and $k_4 = 2$ ps^{-1}, respectively. Recent vibrational echo experiments and molecular dynamics simulations indicate that the frequency correlation function of the OH stretch vibration is characterized by a 50 fs decay and 180 fs beat associated with underdamped intermolecular vibrations of hydrogen bonding partners. Its long-time tail decays exponentially with a time constant of 1.4 ps.[12−14] The short time dynamics are associated with hydrogen bond length fluctuations whereas the longer exponential decay is attributed to the breaking and formation of hydrogen bonds. Accordingly, setting $k_d = (1.4 \text{ ps})^{-1}$, one obtains from eq 7 a value for k_r of 1.24 ps^{-1} which has to be compared with 1.5 ps^{-1} from eq 8. The difference between both values is 20% and is in excellent agreement with observations made in Figure 7. We emphasize again that the model can easily be extended to arbitrary cluster sizes with components, W_i ($i = 0-4$). Using a reasonable averaged distribution of clusters which interconvert with a mean equilibration time, $1/k_d$, of 1.4 ps at room temperature, the conclusions are identical to those drawn from the simpler 2-state model.

D. Comparison with Theoretical Studies. In theoretical studies based on Landau−Teller type formalisms, Rey and Hynes[31,32] and Lawrence and Skinner[29,30] analyzed the relaxation pathway of the excited OH-stretching mode to the ground state. They found that the rate-determining step in the deactivation is the initial transfer from the OH-stretching to the first overtone of the HOD-bending vibration which is facilitated by the solutes internal anharmonicities. Motivated by the experiments of Woutersen et al.[22] Lawrence and Skinner also investigated the temperature dependence of the OH-stretch vibrational relaxation in the range 275−350 K.[30] Since the theory is not able to reproduce the measured lifetimes quantitatively the study was aimed at reproducing relative trends when comparing experiment and theory. These calculations yield a 60% increase of the OH-stretch lifetime of HOD upon heating D_2O from 275 to 350 K whereas an increase of only 20% is observed in the experiment (see Figure 7). At this point, one has to bear in mind that within the theory, the relaxation time is derived from a relatively long (several hundreds of picoseconds) equilibrium molecular dynamics simulation which yields a spectral density of generalized solvent forces acting on the different vibrational modes of the solute. In this way, the Landau−Teller approach produces ensemble averaged rate constants, quite in contrast to the experiment under near ambient conditions, where k_r is reduced by spectral diffusion. Therefore, the calculated values of k_r have to be compared with the ensemble averaged relaxation rates represented in Figure 7 by the straight line. According to this line, a 50% increase of the relaxation time is expected for the temperature range studied in ref 22. Hence, the agreement between our experiment and the theory is much better than it seems at the first glance.

According to the analysis of Lawrence and Skinner,[30] the physical origin of the strong temperature dependence of the relaxation rate arises primarily from variations of the energy gap between the vibrational levels involved, as was suspected before.[28] At elevated temperatures, the energy difference between the first excited OH-stretching state and the first HOD bending overtone is increased and the relaxation decelerates as it becomes more difficult to deposit larger amounts of energy into the solvent. The widening of the energy gap with increasing temperature is mainly caused by a blue shift of the OH-stretching band which overrules a small red-shift of the bending mode. Therefore, the frequency of the OH-stretch absorption maximum

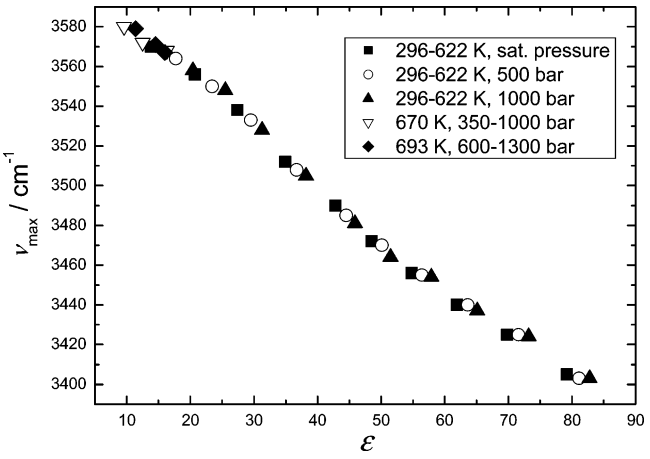

Figure 8. Maximum of the OH-stretch absorption band of HOD vs dielectric constant of water.

ν_{max} of HOD can be considered as a measure of the energy gap. To test whether this mechanism continues to operate upon approaching supercritical conditions, ν_{max} is plotted in Figure 8 vs the dielectric constant of D_2O. As was found before for the vibrational relaxation rate, k_r, there is again a nearly linear $\nu_{max}(\epsilon)$ dependence which points to the importance of the OH-stretch to bend overtone energy gap in determining the vibrational relaxation rate.

Interestingly, Lawrence and Skinner further found that in the temperature range 275−350 K, the change of the spectral density of the fluctuating solvent force acting on the solute vibrational degrees of freedom is only of minor importance for k_r. Since both, shifts of vibrational levels and fluctuating solvent force are expected to linearly correlate with the number of hydrogen bonds per water molecule, it will be very difficult to experimentally differentiate between these two contributions. Nevertheless, the results reported here for the OH-stretch relaxation of HOD in D_2O represent a new challenge for existing theories, which aim at building refined models for liquid water that are capable of describing VER in a quantitative fashion.

5. Conclusions

In summary, we have performed femtosecond mid-infrared pump−probe spectroscopy to explore the dynamics of vibrational relaxation of the OH stretching mode of HOD in D_2O for elevated pressures and temperatures ranging well into the supercritical phase. The density dependence at constant temperature was quantitatively modeled using a binary collision model including an attractive hard sphere interaction between the solute and the solvent. However, the same IBC ansatz failed to explain the temperature dependence for a given solvent density. The breakdown of the IBC approximations was traced back to the simplicity of the solute solvent interaction potential which is unable to adequately represent the evolution of the local density in the first solvation shell with temperature.

Furthermore, a strict correlation was found between the apparent vibrational relaxation rate constant observed experimentally and the density and temperature-dependent dielectric constant of the solvent. Using results from recent molecular dynamics simulations, this correlation can be mapped onto a linear dependence of the relaxation rate constant k_r on the average number of hydrogen bonds in which the solute is engaged. A simple kinetic model that takes into account spectral diffusion through dynamic hydrogen bond breakage and formation reveals that over almost the entire density and temperature range under study, the apparent vibrational relaxation rate is equal to a weighted average (i.e., ensemble average) over cluster-specific relaxation rate constants. This is because under these conditions, spectral diffusion is much faster than energy relaxation thereby blurring the population kinetic of the individual hydrogen-bonded configurations into a unique but averaged relaxation rate.

Not accidentally, at lower temperatures and pressures such as under ambient conditions, this time scale separation does not exist anymore. It is then this complex interplay between spectral diffusion and vibrational relaxation occurring on similar time scale, which is responsible for the fact that different experimental methods failed so far to converge on a unique value for the vibrational relaxation rate in the room-temperature liquid.

Acknowledgment. This paper is dedicated to Prof. Jürgen Troe on the occasion of his 65th birthday. We thank our mentor for his inspirational ability as a teacher of physical chemistry. We consider ourselves fortunate to have enjoyed his fascination for science in the classroom and during our common research. This work was supported by the Deutsche Forschungsgemeinschaft (SFB 357 "Molekulare Mechanismen unimolekularer Reaktionen").

References and Notes

(1) *Ultrafast Infrared and Raman Spectroscopy*; Fayer, M. D., Ed.; Marcel Dekker: New York, 2001.
(2) *Ultrafast hydrogen bonding dynamics and proton-transfer processes in the condensed phase*; Elsaesser, T., Bakker, H. J., Eds.; Kluwer: Dordrecht, The Netherlands, 2002.
(3) Nibbering, E. T. J.; Elsaesser, T. *Chem. Rev.* **2004**, *104*, 1887.
(4) Gale, G. M.; Gallot, G.; Hache, F.; Lascoux, N.; Bratos, S.; Leicknam, J.-C. *Phys. Rev. Lett.* **1999**, *82*, 5211.
(5) Woutersen, S.; Bakker, H. J. *Phys. Rev. Lett.* **1999**, *83*, 2077.
(6) Bratos, S.; Gale, G. M.; Gallot, G.; Hache, F.; Lascoux, N.; Leicknam, J.-C. *Phys. Rev. E* **2000**, *61*, 5211.
(7) Stenger, J.; Madsen, D.; Hamm, P.; Nibbering, E. T. J.; Elsaesser, T. *Phys. Rev. Lett.* **2001**, *87*, 027401.
(8) Stenger, J.; Madsen, D.; Hamm, P.; Nibbering, E. T. J.; Elsaesser, T. *J. Phys. Chem. A* **2002**, *106*, 2341.
(9) Rey, R.; Moller, K. B.; Hynes, J. T. *J. Phys. Chem. A* **2002**, *106*, 11993.
(10) Lawrence, C. P.; Skinner, J. L. *J. Chem. Phys.* **2003**, *118*, 264.
(11) Lawrence, C. P.; Skinner, J. L. *Chem. Phys. Lett.* **2003**, *369*, 472.
(12) Asbury, J. B.; Steinel, T.; Kwak, K.; Corcelli, S. A.; Lawrence, C. P.; Skinner, J. L.; Fayer, M. D. *J. Chem. Phys.* **2004**, *121*.
(13) Corcelli, S. A.; Lawrence, C. P.; Asbury, J. B.; Steinel, T.; Fayer, M. D.; Skinner, J. L. *J. Chem. Phys.* **2004**, *121*, 8897.
(14) Fecko, C. J.; Loparo, J. J.; Roberts, S. T.; Tokmakoff, A. *J. Chem. Phys.* **2005**, *122*, 054506.
(15) Woutersen, S.; Bakker, H. J. *Nature (London)* **1999**, *402*, 507.
(16) Lock, A. J.; Bakker, H. J. *J. Chem. Phys.* **2002**, *117*, 1708.
(17) Larsen, O. F. A.; Woutersen, S. *J. Chem. Phys.* **2004**, *121*, 12143.
(18) Huse, N.; Ashihara, S.; Nibbering, E. T. J.; Elsaesser, T. *Chem. Phys. Lett.* **2005**, *404*, 389.
(19) Cowan, M. L.; Bruner, B. D.; Huse, N.; Dwyer, J. R.; Chugh, B.; Nibbering, E. T. J.; Elsaesser, T.; Miller, R. J. D. *Nature (London)* **2005**, *434*, 199.
(20) Cringus, D.; Lindner, J.; Milder, M. T. W.; Pshenichnikov, M. S.; Vöhringer, P.; Wiersma, D. A. *Chem. Phys. Lett.* **2005**, *408*, 162.
(21) Woutersen, S.; Emmerichs, U.; Bakker, H. J. *Science* **1997**, *278*, 658.
(22) Woutersen, S.; Emmerichs, U.; Nienhuys, H.-K.; Bakker, H. J. *Phys. Rev. Lett.* **1998**, *81*, 1106.
(23) Wang, Z.; Pakoulev, A.; Pang, Y.; Dlott, D. D. *J. Phys. Chem. A* **2004**, *108*, 9054.
(24) Wang, Z.; Pang, Y.; Dlott, D. D. *Chem. Phys. Lett.* **2004**, *397*, 40.
(25) Nienhuys, H.-K.; Woutersen, S.; van Santen, R. A.; Bakker, H. J. *J. Chem. Phys.* **1999**, *111*, 1494.
(26) Laenen, R.; Rauscher, C.; Laubereau, A. *J. Phys. Chem. B* **1998**, *102*, 9304.
(27) Laenen, R.; Rauscher, C.; Laubereau, A. *Phys. Rev. Lett.* **1998**, *80*, 2622.
(28) Gale, G. M.; Gallot, G.; Lascoux, N. *Chem. Phys. Lett.* **1999**, *311*, 123.
(29) Lawrence, C. P.; Skinner, J. L. *J. Chem. Phys.* **2003**, *119*, 1623.
(30) Lawrence, C. P.; Skinner, J. L. *J. Chem. Phys.* **2003**, *119*, 3840.

(31) Rey, R.; Hynes, J. T. *J. Chem. Phys.* **1996**, *104*, 2356.
(32) Rey, R.; Moller, K. B.; Hynes, J. T. *Chem. Rev.* **2004**, *104*, 1915.
(33) Staib, A.; Hynes, J. T. *Chem. Phys. Lett.* **1993**, *204*, 197.
(34) Schwarzer, D.; Troe, J.; Zerezke, M. *J. Chem. Phys.* **1997**, *107*, 8380.
(35) Schwarzer, D.; Troe, J.; Zerezke, M. *J. Phys. Chem. A* **1998**, *102*, 4207.
(36) Myers, D. J.; Chen, S.; Shigeiwa, M.; Cherayil, B. J.; Fayer, M. D. *J. Chem. Phys.* **1998**, *109*, 5971.
(37) Myers, D. J.; Shigeiwa, M.; Fayer, M. D. *J. Phys. Chem. B* **2000**, *104*, 2402.
(38) Kimura, Y.; Yamaguchi, T.; Hirota, N. *Chem. Phys. Lett.* **1999**, *303*, 223.
(39) Bellissent-Funel, M.-C. *J. Mol. Liq.* **2001**, *90*, 313.
(40) Botti, A.; Bruni, F.; Ricci, M. A.; Soper, A. K. *J. Chem. Phys.* **1998**, *109*, 3180.
(41) Boero, M.; Terakura, K.; Ikeshoji, T.; Liew, C. C.; Parrinello, M. *Phys. Rev. Lett.* **2000**, *85*, 3245.
(42) Boero, M.; Terakura, K.; Ikeshoji, T.; Liew, C. C.; Parrinello, M. *J. Chem. Phys.* **2001**, *115*, 2219.
(43) Kohl, W.; Lindner, H. A.; Franck, E. U. *Ber. Bunsen-Ges. Phys. Chem.* **1991**, *95*, 1586.
(44) Amita, F.; Okada, K.; Oka, H.; Kajimoto, O. *Rev. Sci. Instrum.* **2001**, *72*, 3605.
(45) PROPATHGroup. *PROPATH: A Program Package for Thermophysical Properties, Version 12.1*, 2001.
(46) Franck, E. U.; Roth, K. *Discuss. Faraday Soc.* **1967**, *43*, 108.
(47) Gorbaty, Y. E.; Kalinichev, A. G. *J. Phys. Chem.* **1995**, *99*, 5336.
(48) Bakker, H. J.; Nienhuys, H.-K.; Gallot, G.; Lascoux, N.; Gale, G. M.; Leicknam, J.-C.; Bratos, S. *J. Chem. Phys.* **2002**, *116*, 2592.
(49) English, N. J. *Mol. Phys.* **2005**, *103*, 1945.
(50) Chesnoy, J.; Gale, G. M. *Ann. Phys. Fr.* **1984**, *9*, 893.
(51) Davis, P. K.; Oppenheim, I. *J. Chem. Phys.* **1972**, *57*, 505.
(52) Einwohner, T.; Alder, B. J. *J. Chem. Phys.* **1968**, *49*, 1458.
(53) Potoff, J. J.; Panagiotopoulos, A. Z. *J. Chem. Phys.* **1998**, *109*, 10914.
(54) Teubner, M.; Schwarzer, D. *J. Chem. Phys.* **2003**, *119*, 2171.
(55) Delalande, C.; Gale, G. M. *J. Chem. Phys.* **1979**, *71*, 4804.
(56) Allen, M. P.; Tildesley, D. J. *Computer simulation of liquids*; Clarendon Press: Oxford, England, 1996.
(57) Vikhrenko, V. S.; Schwarzer, D.; Schroeder, J. *Phys. Chem. Chem. Phys.* **2001**, *3*, 1000.
(58) Winkler, K.; Lindner, J.; Vöhringer, P. *Phys. Chem. Chem. Phys.* **2002**, *4*, 2144.
(59) Kalinichev, A. G.; Bass, J. D. *Chem. Phys. Lett.* **1994**, *231*, 301.
(60) Yoshii, N.; Miura, S.; Okazaki, S. *Chem. Phys. Lett.* **2001**, *345*, 195.
(61) Yoshii, N.; Yoshie, H.; Miura, S.; Okazaki, S. *J. Chem. Phys.* **1998**, *109*, 4873.